90 days of age. Calcium deposits were extensive throughout the entire sections of high-Pi fed mdx mice at 90 days of age.

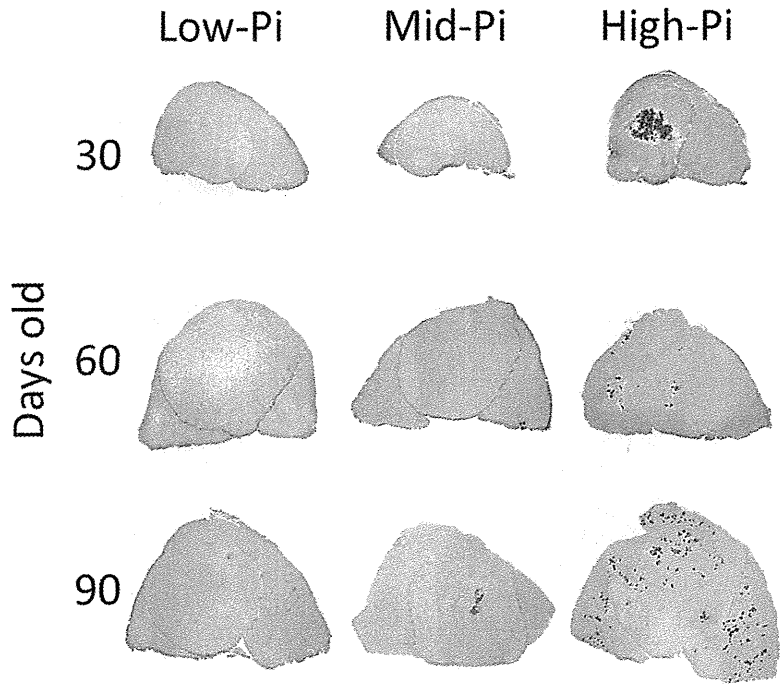

Fig. 5. Alizarin red S-stained cryosections of mdx mice quadriceps muscle. Calcium deposits are stained red.

5.2 Ectopic calcification in other tissues

Although the presence of calcification is rarely reported in organs of mdx mice other than skeletal muscle, including the heart and kidneys, these mice exhibit abnormal cardiac pathology and function (Zhang et al., 2008) and their myocardium is vulnerable (Costas et al., 2010). Rodent models of muscular dystrophies may have potential for sensitivity to myocardial calcification when challenged by mechanical or chemical stressors, because such calcification is commonly observed in the hamster model of muscular dystrophy (Burbach, 1987). For instance, Elsherif et al. (2008) found that dystrophin and β1 integrin double-knockout mice (β1KOmdx) show exacerbated myocardiopathy and extensive calcification in the heart, particularly under pregnancy-induced stress. Thus we predicted that high-Pi intake would also affect calcification in the myocardium of mdx mice.

Calcification in the heart was evaluated by 8 μm cryosections of samples from the three Pi-diet group mice. We found that high-Pi intake induced relatively few cases of myocardial calcification in mdx mice at both 60 and 90 days of age (4 of 30 samples). The form of the crystallization observed in the heart was similar to that of myofiber calcification, although the amount was considerably less (Fig. 6A, C). The incidence of calcification in the heart was absent in mdx fed mid-Pi or low-Pi diets. None of B10 mice fed any of the three types of phosphate diets exhibited myocardial calcification.

As previously described, klotho mutant mice display a number of age-related diseases, including soft tissue calcification. Morishita et al. (2010) reported that klotho mice fed a normal diet show kidney calcification, whereas mice fed a low-Pi diet have reduced precipitation of calcium in the kidneys. We found that a high-Pi intake results in slight ectopic calcification in kidneys of mdx mice (Fig. 6B, D) whereas mdx mice fed mid-Pi or low-Pi diets showed no evidence of calcium deposition in the kidneys. Similar to the findings in the heart, B10 mice under all phosphate diets also showed no calcification in the kidneys.

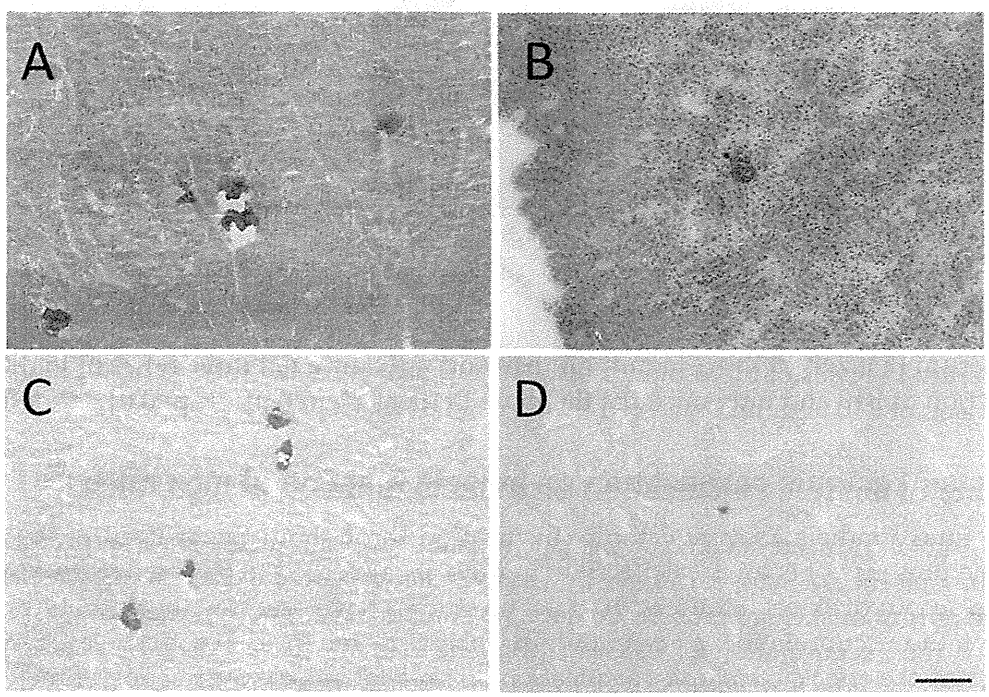

Fig. 6. H&E and alizarin red S-stained cryosections of the heart and kidneys of an mdx mouse fed a high-Pi diet. H&E-stained cryosections of the heart (A) and kidney (B). Alizarin red S-stained cryosections of the heart (C) and kidney (D). The bar represents 100 μm.

5.3 Changes in serum biochemistry

We also examined the serum calcium and phosphate concentrations of B10 and mdx mice fed the three types of Pi diets. The serum phosphate levels of high-Pi fed mdx mice were significantly higher than those of B10 mice fed the same diet, and mdx mice under mid-Pi and low-Pi diets (Fig. 7). However, no marked differences in serum calcium concentrations of mdx mice were detect in the different diet groups. Serum phosphate concentration is largely influenced by dietary intake, with the over-consumption of phosphate often resuting to cause hyperphosphatemia (Calvo et al., 1994), secondary hyperparathyroidism with bone re-sorption (Lutwak et al., 1975), and bone loss (Draper et al., 1979). It is likely that high phosphate intake leads to overworked kidneys and a reduced rate of calcium and phosphate filtration.

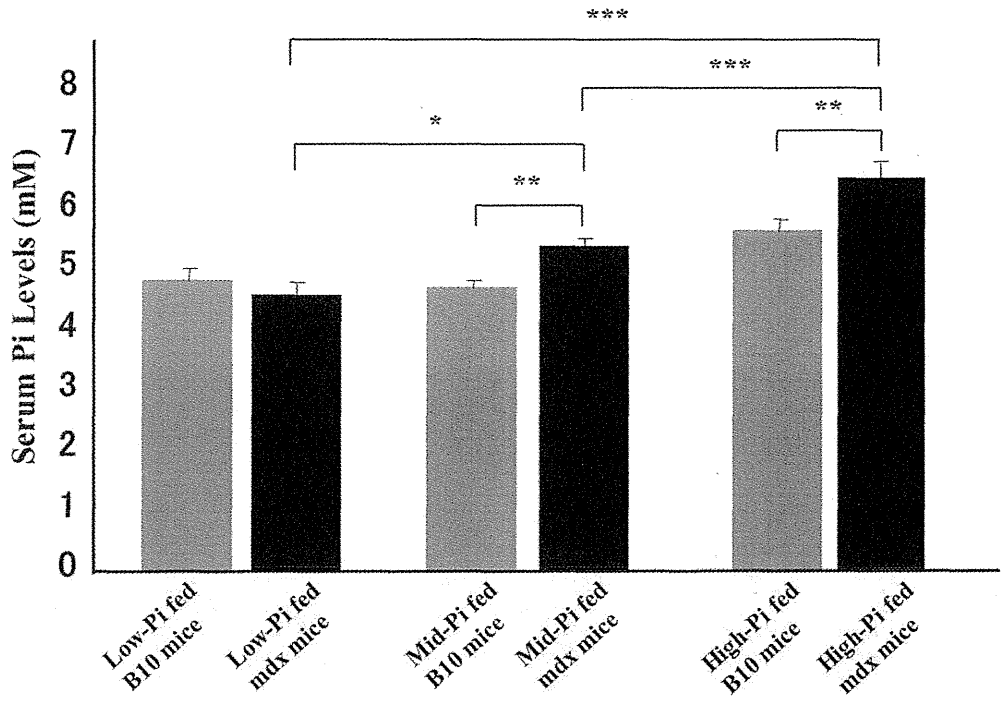

Fig. 7. Serum Pi levels of three-month-old B10 and mdx mice fed three types of Pi diets. Comparison of B10 and mdx mice fed the three Pi diets. (*: $p<0.05$; **: $p<0.01$; ***: $p<0.001$).

6. Effects of ectopic calcification on muscle function of mdx mice

High-Pi intake induced severe ectopic calcification throughout the skeletal muscle of mdx mice. The presence of ectopic calcification in muscles appeared to have a negative impact on the force output of skeletal muscle. To date, no studies have reported the pathophysiological effects of the accumulation of calcium phosphate in muscles. For this reason, we have investigated the effects of ectopic calcification on skeletal muscle contraction of mdx mice.

For muscle force measurements, *in situ* maximal isometric twitch force and tetanic force of right triceps surae muscle (TSM) were recorded. The isometric force recording system was custom-made and the experimental protocols were based on the design of Dorchies et al. (2006). Sixty-day-old B10 and mdx mice fed the three phosphate diets were lightly anesthetized by diethylether gas and then immobilized on a cork board by covering the bodies with Novix-II (Asahi Techno Glass, Chiba, Japan). A confined area of skin and myofasia of the right hindlimb was cut and exposed, and the sciatic nerve was dissected to induce the analgesic conditions. The knee joint was firmly immobilized by a needle that served as the fulcrum and the Achilles tendon of the leg was then severed and connected to a platinum electrode clip associated with a force transducer (DS2-50N Digital Force Gauge; Imada, Aichi, Japan). A second platinum electrode was directly inserted into the TSM. Experimental trials were started after the animals recovered from anesthesia. Using this procedure, we avoided negative effects (*i.e.* muscle relaxation) of the anesthetic regimen, which we previously confirmed and were able to collect real data without any disturbances. For the measurement of maximal single twitch, muscles were stimulated with a square wave pulse (0.5-msec duration) of stimulation voltage. Tetanic force was measured with 200-msec bursts of frequency set to 100 Hz. Muscle length and weight of TSM were measured to estimate the cross-sectional area

(CSA) of the muscle (in mm^2). The specific twitch and tetanic force were normalized by dividing the measured force by the CSA. Using manual settings of the optimal muscle length, maximal twitch contractions were measured within trials up to 20 contractions and all tetanic force measurements were made at locations where the single twitch force was the greatest.

6.1 Results of maximal single force (MSF) and maximal tetanic force (MTF) measurements

Pre-tests results revealed that B10 mice fed the normal CE-2 diet had significantly stronger maximal single force in response to single-pulse stimulation than that of mdx mice (data not shown). This result is consistent with a previous study by Dorchies et al. (2006). Furthermore, although mdx mice have a heavier body weight and muscle mass of the TSM, they exhibited weaker muscle force compared with the control mice. This finding was also consisted with that reported previously (Quinlan et al., 1992), although the muscle mass of anterior tibial muscle was compared, rather than TSM. Therefore, we are confident that our isometric force recording system can be used to evaluate and compare muscle forces between B10 and mdx mice fed the different phosphate diets (Table 1).

We did not detect any significant differences in twitch force between B10 mice of the three phosphate diets groups. However, the high-Pi diet mdx mice had significantly lower ($p<0.001$) single force than that of mdx mice fed a mid-Pi diet (Fig. 8A), while maximal single force was significantly higher in mdx mice fed a low-Pi diet compared with mid-Pi diet mdx mice. Notably, however, this value was still lower (25% less) than the corresponding value of B10 mice fed a low-Pi diet.

The maximal tetanic force in response to burst stimulation was also measured for all mice. Similar to the results of twitch force, B10 mice had significantly higher tetanic force than mdx mice for all three phosphate diets, whereas no marked differences were detected among B10 mice. Mdx mice fed a high-Pi diet produced significantly less ($p<0.001$) tetanic force than the other mdx mice (Fig. 8B). Based on these findings, we conclude that high-Pi diet has a greater influence on generating the tetanic force in mdx mice than producing twitch force. These results strongly suggest that calcium deposits in muscles interfere with muscle function. The improvement of muscle forces was likely due to the reduction of ectopic calcification because low Pi-diet did not have a positive effect on force generation in B10 mice, which have no ectopic calcification. However, it is also likely that other factors related to dietary phosphate restriction also contribute to improving muscle function.

Mouse	#	Weight (g)	MSF (mN/mm^2)	MTF (mN/mm^2)
Low-Pi B10	7	23.1±1.0	102.5±4.6	344.8±15.2
Low-Pi mdx	7	23.8±1.4	74.2±2.4	254.9±14.6
Mid-Pi B10	7	22.3±0.7	100.0±4.1	341.0±11.1
Mid-Pi mdx	7	25.2±0.5	66.8±1.5	246.4±7.2
High-Pi B10	7	22.8±0.7	101.0±3.3	335.6±6.3
High-Pi mdx	7	23.6±0.7	59.6±2.0	193.9±9.6

Table 1. Results of MSF and MTFmeasurements of B10 and mdx mice for the three Pi diet conditions.

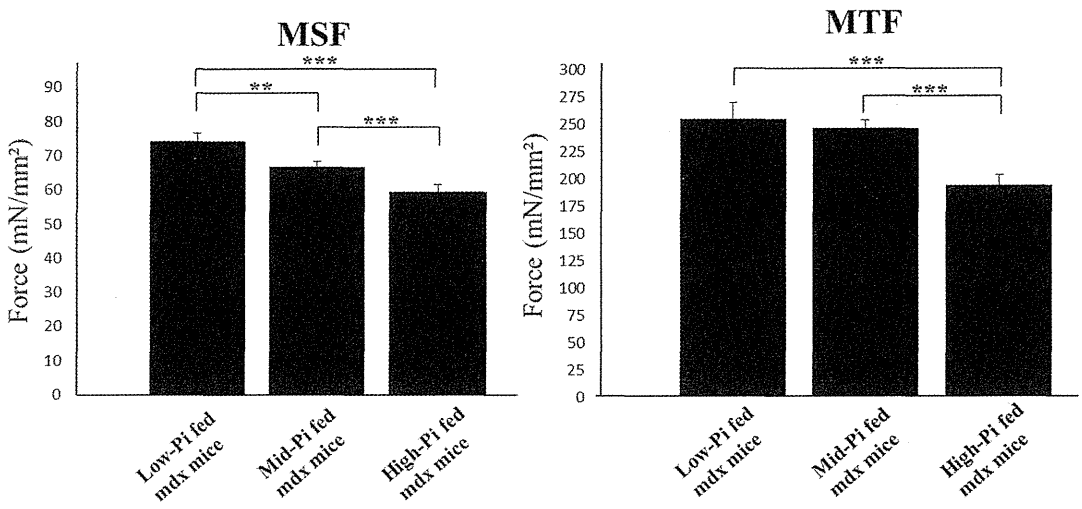

Fig. 8. MSF and MTF measurements of mdx mice for the three Pi diet conditions. (A) Results of MSF. (B) Results of MTF (**: $p<0.01$; ***: $p<0.001$).

7. Reduced calcification by low Pi diet in a longitudinal study

Although the influence of dietary phosphate intake on the precipitation of calcium in mdx mice skeletal muscles has been clarified, the effects of phosphate restriction on severe ectopic calcification remained unclear. To understand the impact of phosphate restriction on the deposition of calcium, a longitudinal study was conducted for four mdx mice raised on high-Pi diet from weaning to 60 days of age. At age of 60 days, whole-body images of the mdx mice were taken by noninvasive CT scanning using a Latheta LTC-200 X-ray micro CT scanner (Hitachi Aloka Medical, Tokyo, Japan) (Fig. 9). The mdx mice were then divided into two groups, a continuously fed high-Pi diet group and a low-Pi diet group, until the age of 90 days, at which point whole-body images of the mice were taken again. The whole-body images and volume density of ectopic calcification in the lower body (from the top of os coxae to ankle joint) were compared (Fig. 10). Mice fed a high-Pi diet displayed an increased volume (0.066 cm^3) of ectopic calcification from 60 to 90 days of age, whereas mdx mice fed a low-Pi diet had a reduced (-0.007 cm^3). Thus, it was concluded that the restriction the restriction of dietary phosphate from the age of 60 days reduced the pre-formed ectopic calcification within one month, while continuously feeding the mice a high-Pi diet led to more severe calcium deposits.

8. Mechanisms of calcification

The complete mechanism underlying progressive muscle degeneration due to dystrophin deficit is unclear. Dystrophin-deficient muscles are highly susceptible to the oxidative stress that results from the early onset of muscle degeneration. Muscle necrosis actively occurs following the degeneration, leading to fibrosis and calcification of muscle fibers (Vercherat et al., 2009). It has been suggested that vascular calcification is actively regulated by osteogenic gene expression in vascular smooth muscle cells (Giachelli, 1999). Attention has been focused on inorganic phosphate as one of the potential factors regulating the observed cellular phenotypic changes, as smooth muscle cells *in vitro* cultured under high-Pi conditions undergo osteogenesis and form calcium deposits (Jono et al., 2000). As skeletal muscle satellite cells possess multilineage potential (Asakura et al., 2001; Wada et al., 2002), they might also undergo osteogenic differentiation under high-Pi conditions.

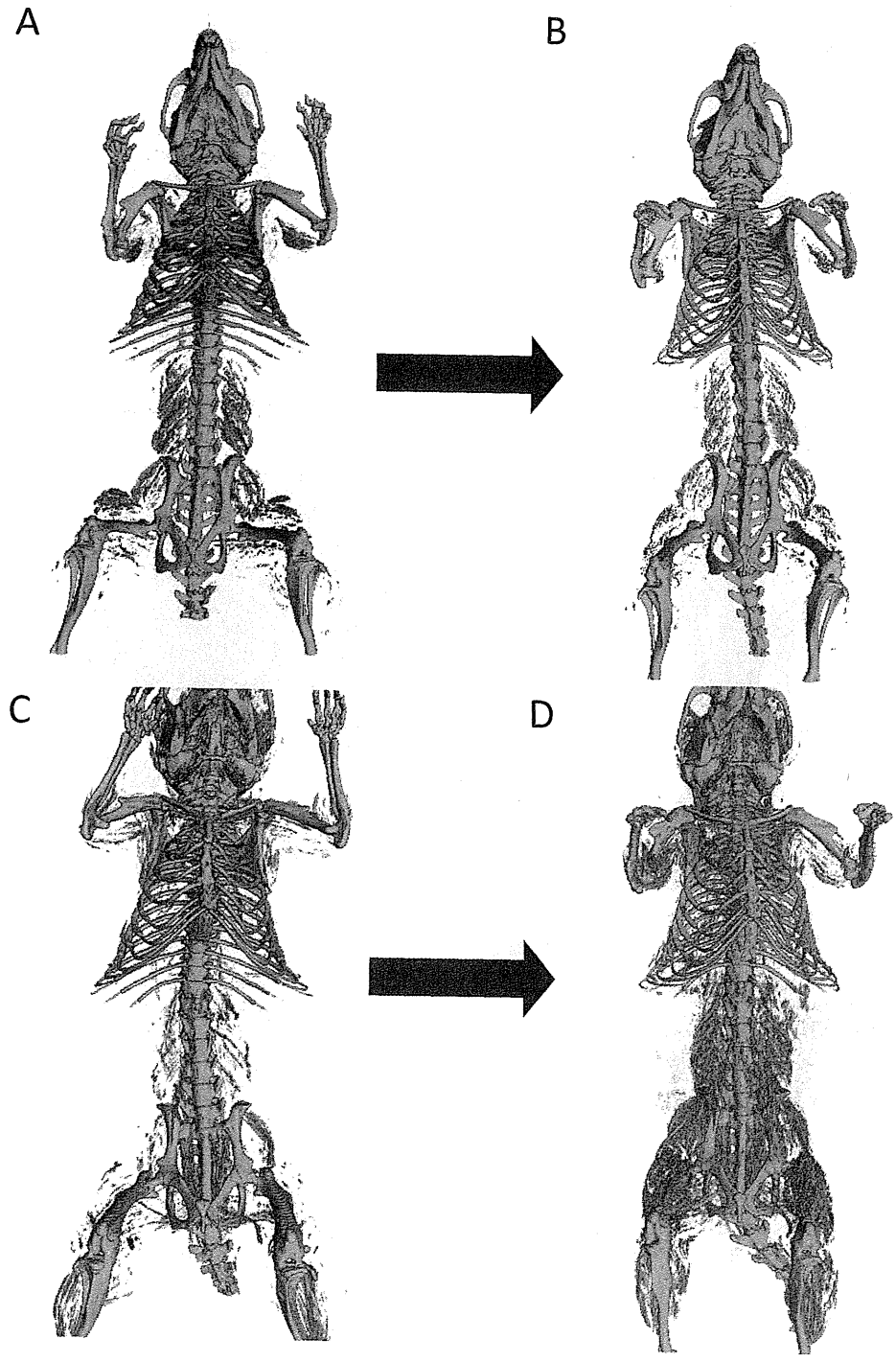

Fig. 9. 3D images of 60-day-old mdx mice fed a high-Pi diet (left) and the images of the same mice after 30 days (A,C) Sixty-day-old mdx mice fed a high-Pi diet. (B) The same mdx mice (90-day-old) fed a low-Pi diet for 30 days. (D) The same mdx mice (90-day-old) fed a high-Pi diet for 30 days. Bones are shown in grey and ectopic calcification is in light blue.

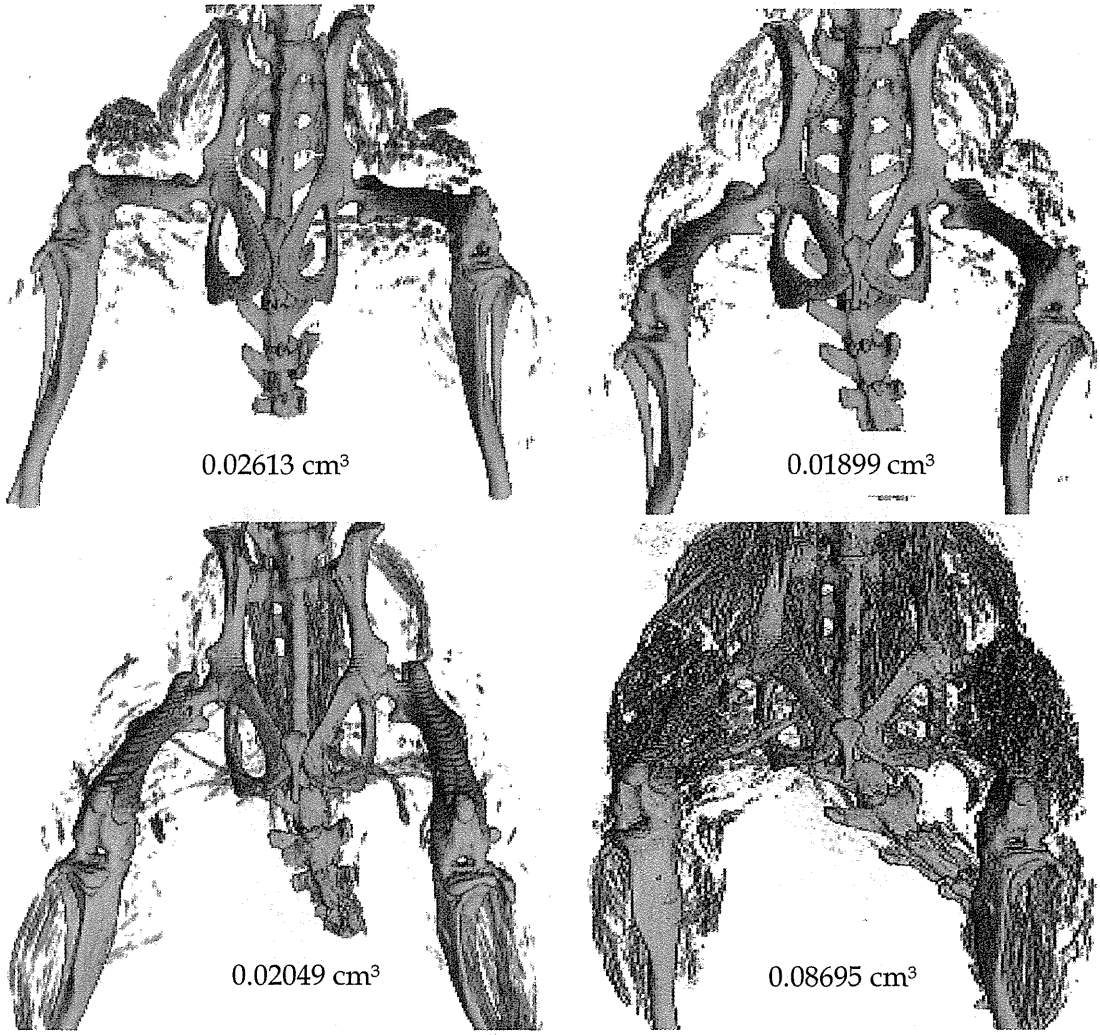

Fig. 10. Enlarged 3D images of the lower limbs of mdx mice fed a high-Pi diet (left) and the images of the same mice fed either low-Pi (top right) or high-Pi diets (bottom right) for 30 days. The numbers represent the volume densities of ectopic calcification in the lower body (from the top of os coxae to ankle joint).

8.1 Pi-induced osteogenesis and reduced myogenesis in C2C12 cells

To study the effects of Pi on muscle cell differentiation, murine myoblast-derived C2C12 cells were cultured for four days under various Pi concentrations and then immunostained for the presence of myogenic (myosin heavy chain; MyHC) and osteogenic (Matrix Gla Protein; MGP) markers. When cultured in normal differentiation medium (Pi=1 mM), the cells underwent muscle differentiation and formed myotubes. Myogenesis proceeded until the Pi concentration of the differentiation medium reached 5 mM, while myotube formation was strongly suppressed at 7 mM. (Fig. 11).

The expression of Runx2, a transcription factor of osteogenesis, increased with the rise of the Pi concentration (Fig. 12A). The retardation of myogenesis caused by the high Pi concentration was also evident by the decrease in both the fusion index and myogenin

expression (Fig. 12A). It was notable that in medium containing 5 mM Pi, myogenesis was not inhibited and the C2C12 cells differentiated into myotubes, while the expression Runx2 was augmented (Fig. 12B). Further observation revealed that myogenin and Runx2 did not colocalize in the nuclei of myotubes, rather, Runx2 was localized in the cytoplasm. This finding suggests that Runx2 is inactive in myogenic cells, as it has been reported that Runx2 activity is regulated by translocation between the nucleus and cytoplasm (Zaidi et al., 2001). Upregulation of Runx2 expression was observed by Western blotting not only when the C2C12 cells were cultured under high-Pi conditions, but also when cultured in the presence of calcium deposits, which were generated by the addition of sodium phosphate and calcium chloride to the medium (Fig. 12C). Osteocalcin, another osteogenic marker which is a secreted protein whose expression is regulated by Runx2, was also examined (Fig 12D). RT-PCR was performed with RNA samples prepared from C2C12 cells cultured under the various Pi concentrations for four days. Osteocalcin expression was undetectable when the cells were cultured with 1 mM Pi, but increased with the elevation of the Pi concentration. We also measured calcium deposition in C2C12 cells cultured under the various Pi concentrations and found that although the cells did not deposit calcium under normal Pi conditions, cells cultured in medium containing 3 mM Pi or higher deposited calcium (alizarin red S-positive cells; Fig. 12E). The amount of calcium deposits increased significantly at higher Pi concentrations.

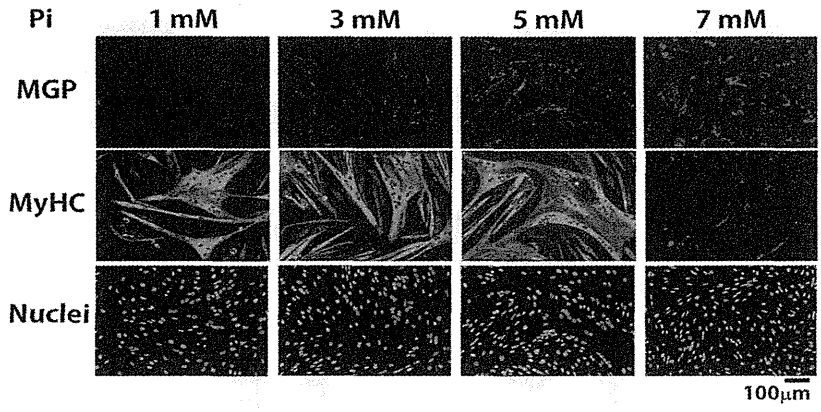

Fig. 11. Immunocytochemistry of C2C12 cells cultured under various Pi concentrations. Cells were immunostained for MyHC (green), MGP (red), and nuclei (blue).

8.2 Pi-induced calcification in primary cultures of skeletal muscle cells

Cells isolated from mdx skeletal muscle tissue were cultured in normal Pi (1.3 mM) to high-Pi (5 mM) medium to study the effects of Pi in primary culture cells. The cells formed myotubes when cultured in normal medium, whereas myotube formation was strongly inhibited under high-Pi conditions. The results of both alizarin red S and von Kossa staining revealed that numerous calcium deposits were present in cells after ten days of culture in high-Pi medium, but none detected in cells cultured in normal medium (Fig. 13). Therefore, Pi induces osteogenesis in myoblasts, resulting in calcification while inhibiting myogenesis. We conclude that the calcification of skeletal muscle is mainly due to the elevation of intracellular Pi levels.

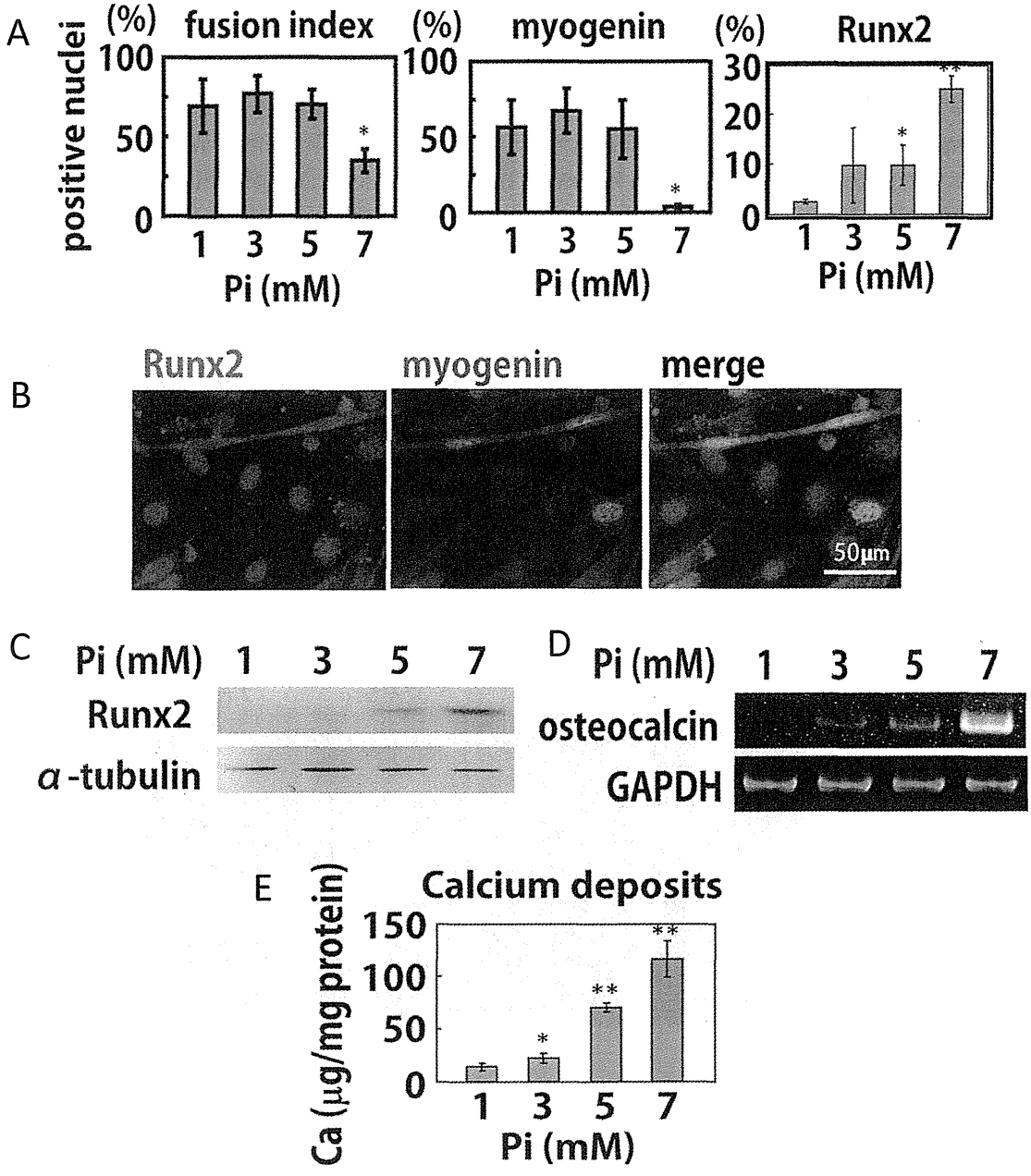

Fig. 12. Immunocytochemistry and RT-PCR of C2C12 cells cultured under various Pi concentrations (1, 3, 5, and 7 m). (A) The fusion index, myogenin expression, and expression of Runx2 were quantified. The fusion index and ratio of nuclei expressing myogenin decreased, while the ratio of Runx2-expressing nuclei increased with increasing Pi concentration. (B) Close observation of cells cultured in medium containing 5 mM Pi by staining with Hoechst 33258 to show the nuclei, or immunostained for myogenin or Runx2. (C) Western blotting of C2C12 cells cultured under increased Pi or Ca concentrations. (D) RT-PCR for osteocalcin in C2C12 cells cultured under various Pi concentrations. (E) Quantification of calcium deposites generated by C2C12 cells cultured under various Pi concentrations. (*: $p<0.05$; **: $p<0.01$).

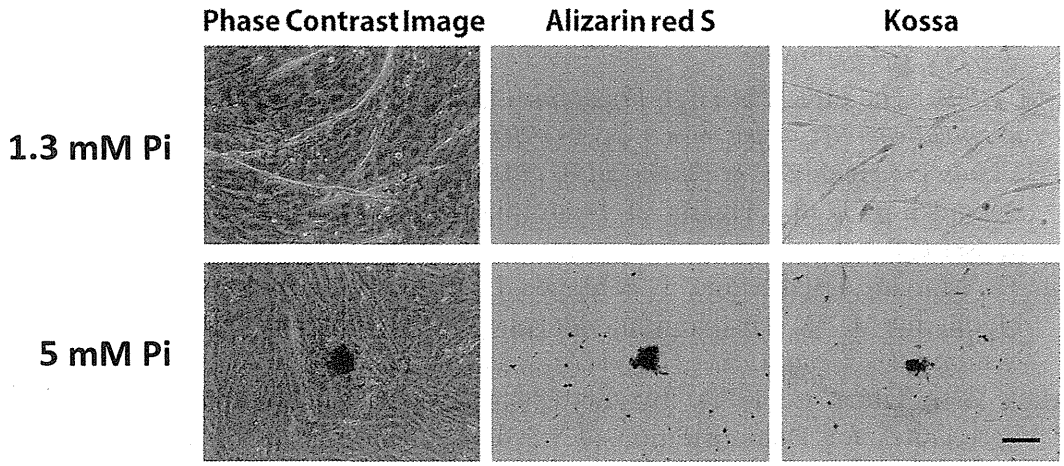

Fig. 13. Calcification of mdx mouse muscle-derived primary culture cells. Calcium deposits were stained red or black with alizarin red S and von Kossa staining, respectively. No calcification was observed when cells were cultured in normal medium containing 1.3 mM Pi. The von Kossa-stained samples were counterstained with nuclear fast red, and myotubes appear pink. The bar represents 100μm.

9. Conclusion

In this study, we reviewed the mechanisms underlying calcification in skeletal muscle cells following the elevation of intracellular Pi concentrations and revealed the effects of dietary phosphate intake on ectopic calcification in mdx mice. Both *in vivo* and *in vitro*, high-Pi conditions lead to the precipitation of calcium in mdx mice. We have demonstrated that the presence of ectopic calcification in skeletal muscle exacerbates the impaired muscle function of mdx mice, which represents a novel finding. The main goal of our studies is to understand the effects and efficacy of nutritional components on muscular dystrophy as a prior therapy. The effects of dietary phosphate intake on muscle pathology and kidney function need to further elucidated in future studies. Furthermore, the therapeutic potential of nutrition, particularly phosphate intake, should be considered when treating patients with DMD.

10. Acknowledgement

This work has been supported by Health and Labour Sciences Research Grant (19A-020) for Research on Psychiatric and Neurological Diseases and Mental Health, Intramural Research Grant(23-5) for Neurological and Psychiatric Disorders of NCNP and a Research Grant for Nervous and Mental Disorders [20B-13] from the Ministry of Health, Labour and Welfare, Japan.

11. References

Asakura, A.; Komaki, M. & Rudnicki, M. (2001). Muscle Satellite Cells are Multipotential Stem Cells that Exhibit Myogenic, Osteogenic, and Adipogenic Differentiation. Differentiation, Vol.68, pp.245-253.

Burbach, J. (1987). Ultrastructure of Cardiocyte Degeneration and Myocardial Calcification in the Dystrophic Hamster. *The American Journal of Anatomy*, Vol.179, pp.291-307.

Calvo, M. (1994). The Effects of High Phosphoru Intake on Calcium Homeostasis. *Advances in Nutritional Researches*, Vol.9, pp.183-207.

Costas, J.; Nye, D.; Henley, J. & Plochocki, J. (2010). Voluntary Exercise Induces Structural Remodeling in the Hearts of Dystrophin-deficient Mice. *Muscle Nerve*, Vol.42, pp.881-885.

Coulton, G.; Morgan, J.; Partridge, T. & Sloper, J. (1988). The mdx Mouse Skeletal Muscle Myopathy: I. A Histological, Morphometric and Biochemical Investigation. *Neuropathology and Applies Neurobiology*, Vol.14, pp.53-70.

Dingerkus, G. & Uhler, L. (1977). Enzyme Clearing of Alcian Blue Stained Whole Small Vertebrates for Demonstration of Cartilage. *Biotechnic & Histochemistry*, Vol.52, pp.229-232.

Dorchies, O.; Wagner, S.; Vuadens, O.; Waldhauser, K.; Buetler, T.; Kucera, P. & Ruegg, U. (2006). Green Tea Extract and Its Major Polyphenol(-)-epigallocatechin Gallate Improve Muscle Function in a Mouse Model of Duchenne Muscular Dystrophy. *American Journal of Physiology. Cell Physiology*, Vol.290, pp.616-625.

Draper, H. & Bell, R. (1979). Nutrition and Osteoporosis. *Advances in Nutritional Researches*, Vol.145, pp.389-391.

El-Abbadi, M.; Pai, A.; Leaf, E.; Yang, H.; Bartley, B.; Quan, K.; Ingalls, C.; Liao, H. & Giachelli, C. (2009). Phosphate Feeding Induces Arterial Medial Calcification in Uremic Mice: Role of Serum Phosphorus, Fibroblast Growth Factor-23, and Osteopontin. *Kidney International*, Vol.75, pp.1297-1307.

Elsherif, L.; Huang, M.; Shai, S.; Yang, Y.; Li, R.; Chun, J.; Mekany, M.; Chu, A.; Kaufman, S. & Ross, R. (2008). Combined Deficiency of Dystrophin and β1 Integrin in Cardiac Myocyte Causes Myocardial Dysfunction, Fibrosis and Calcification. *Circulation Research*, Vol.102, pp.1109-1117.

Gaschen, F.; Hoffman, E.; Gorospe, J.; Uhl, E.; Senior, D.; Cardinet, G. & Pearce, L. (1992). Dystrophin Deficiency Causes Lethal Muscle Hypertrophy in Cats. *Journal of the Neurological Sciences*, Vol.110, pp.149-159.

Giachelli, C. (2009). The Emerging Role of Phosphate in Vascular Calcification. Kidney International, V0l75, pp.890-897.

Hu, M.; Kuro-o,M. & Moe, O. (2010). Klotho and Kidney Disease. *Journal of Nephrology*, Vol.16, pp.136-144.

Kendrick, J.; Kestenbaum, B. & Chonchol, M. (2011). Phosphate and Cardiovascular Disease. *Advances in Chronic Kidney Disease*, Vol.18, pp.113-119.

Khan, M. (1993). Corticosteroid Therapy in Duchenne Muscular Dystrophy. *Journal of the Neurological Sciences*, V0l.120, pp.8-14.

Kikkawa, M.; Ohno, T.; Nagata, Y.; Shiozuka, M.; Kogure, T. & Matsuda, R. (2009). Ectopic Calcification is Caused by Elevated Levels of Serum Inorganic Phosphate in Mdx Mice. *Cell Structure and Function*, Vol.34, pp.77-88.

Korff, S.; Riechert, N.; Schoensiegel, F.; Weichenhan, D.; Autschbach, F.; Katus, H. & Ivandic, B. (2006). Calcification of Myocardial Necrosis is Common in Mice. *Virchows Archiv*, Vol.448, pp.630-638.

Kuro-o. (2010). Overview of the FGF-23-Klotho Axis. *Pediatric Nephrology*, Vol.25, pp.583-590.

Kuro-o, M.; Matsumura, Y.; Aizawa, H.; Kawaguchi, H.; Suga, T.; Utsugi, T.; Ohyama, Y.; Kurabayashi, M.; Kaname, T.; Kume, E.; Iwasaki, H.; Iida, A.; Shiraki-Iida, T.; Nishikawa, S.; Nagai, R. & Nabeshima, Y. (1997). Mutation of the Mouse *Klotho* Gene Leads to a Syndrome Resembling Ageing. *Nature*, Vol.309, pp.45-51.

Liu, J.; Okamura, C.; Bogan, D.; Bogan, J.; Childers, M. & Kornegay. J. (2004). Effects of Prednisone in Canine Muscular Dystrophy. *Muscle Nerve*, Vol.30, pp.767-773.

Lutwak, L. (1975). Metabolic and Biochemical Considerations of Bone. *Annals of Clinical and Laboratory Science*, Vol.5, pp.185-194.

Matsuda, R.; Nishikawa, A. & Tanaka, H. (1995). Visualization of Dystrophic Muscle Fibers in Mdx Mouse by Vital Staining with Evans Blue: Evidence of Apoptosis in Dystrophin-Deficient Muscle. *Journal of Biochemistry*, Vol.118, pp.959-964.

McLeod, M. (1980). Differential Staining of Cartilage and Bone in Whole Mouse Fetuses by Alcian Blue and Alizarin Red S. *Teratology*, Vol.22, pp.229-301.

Morishita, K.; Shirai, A.; Kubota, M.; Katakura, Y.; Nabeshima, Y.; Takeshige, K. & Kamiya, T. (2010). The Progression of Aging in *Klotho* Mutant Mice Can Be Modified by Dietary Phosphorus and Zinc. *The Journal of Nutrition*, Vol.131, pp.3182-3188.

Nguyen, F.; Cherel, L.; Guigand, I.; Goubault-Leroux & Myers, M. (2002). Muscle Lesions Associated with Dystrophin Deficiency in Neonatal Golden Retriver Puppies. *Journal of Comparative Pathology*, Vol.126, pp.100-108.

Quinlan, J.; Johnson, S.; McKee, M. & Lyden, S. (1992). Twitch and Tetanus in mdx Mouse Muscle. *Muscle Nerve*, Vol.15, pp.837-842.

Razzaque, M.; Sitara, D.; Taguchi, T.; St-Arnaud, R. & Lanske, B. (2006). Premature Aging-like Phenotype in Fibroblast Growth Factor 23 Null Mice is a Vitamin D Mediated Process. *The FASEB Journal*, Vol.20, pp.720-722.

Vercherat, C.; Chung, T.; Yalcin, S.; Gulbagci, N.; Gopinadhan, S.; Ghaffari, S. & Taneja, R. (2009). Stra13 Regulates Oxidative Stress Mediated Skeletal Muscle Degeneration. *Human Molecular Genetics*, Vol.18, pp.4304-4316.

Verma, M.; Asakura, Y.; Hirai, H.; Watanabe, S.; Tastad, C.; Fong, G.; Ema, M.; Call, J.; Lowe, D. & Asakura, A. (2010). *Fit-1* Haploinsufficiency Ameliorates Muscular Dystrophy Phenotype by Developmentally Increased Vasculature in Mdx Mice. *Human Molecular Genetics*, Vol.19, pp.4145-4159.

Wada, M.; Inagawa-Ogashiwa, M.; Shimizu, S.; Yasumoto, S. & Hashimoto, N. (2002). Generation of Different Fates from Multipotent Muscle Stem Cells. *Development*, Vol.129, pp.2987-2995.

Webb, G. & Byrd, R. (1994). Simultaneous Differential Staining of Cartilage and Bone in Rodent Fetuses: an Alcian Blue and Alizarin Red S Procedure Without Glacial Acetic Acid. *Biotechnic and Histochemistry*, Vol.64, pp.181-185.

Wong, B. & Christopher, C. (2002). Corticosteroids in Duchenne Muscular Dystrophy: a Reappraisal. *Journal of Child Neurology*, Vol.17, pp.183-190.

Zaidi, S.; Javed, A.; Choi, J.; van Wijnen, A.; Stein, J.; Lian, J. & Stein, G. (2001). A Specific Targeting Signal Directs Runx2/Cbfa1 to Subnuclear Domains and Contributes to Transactivation of the Osteocalcin Gene. *Journal of Cell Sciences*, Vol.114, pp.3093-3102.

Zhang, W.; Hove, M.; Schneider, J.; Stuckey, D.; Sebag-Montefiore, L.; Bia, B.; Radda, G.; Davis, K.; Neubauer, S. & Clarke, K. (2008). Abnormal Cardiac Morphology, Function and Energy Metabolism in the Dystrophic mdx Mouse: An MRI and MRS Study. *Journal of Molecular and Cellular Cardiology*, Vol.45, pp.754-760.

Psychiatry Research: Neuroimaging 212 (2013) 79–87

Contents lists available at SciVerse ScienceDirect

Psychiatry Research: Neuroimaging

journal homepage: www.elsevier.com/locate/psychresns

Correlation between prefrontal cortex activity during working memory tasks and natural mood independent of personality effects: An optical topography study

Ryuta Aoki [a,b], Hiroki Sato [c,*], Takusige Katura [c], Ryoichi Matsuda [a], Hideaki Koizumi [c]

[a] Department of Life Sciences, Graduate School of Arts and Sciences, The University of Tokyo, 3-8-1 Komaba, Meguro-ku, Tokyo 153-8902, Japan
[b] Japan Society for the Promotion of Science, 8 Ichibancho, Chiyoda-ku, Tokyo 102-8472, Japan
[c] Hitachi, Ltd., Central Research Laboratory, 2520 Akanuma, Hatoyama, Saitama 350-0395, Japan

ARTICLE INFO

Article history:
Received 4 February 2012
Received in revised form
24 August 2012
Accepted 11 October 2012

Keywords:
Near-infrared spectroscopy (NIRS)
Profile of Mood States (POMS)
NEO Five-Factor Inventory (NEO-FFI)
Behavioral Inhibition/Activation Systems (BIS/BAS)

ABSTRACT

Interactions between mood and cognition have drawn much attention in the fields of psychology and neuroscience. Recent neuroimaging studies have examined a neural basis of the mood–cognition interaction that which emphasize the role of the prefrontal cortex (PFC). Although these studies have shown that natural mood variations among participants are correlated with PFC activity during cognitive tasks, they did not control for personality differences. Our aim in this study was to clarify the relationship between natural mood and PFC activity by partialling out the effects of personality. Forty healthy adults completed self-report questionnaires assessing natural mood (the Profile of Mood States) and personality (the NEO Five-Factor Inventory and the Behavioral Inhibition/Activation Systems scales). They performed verbal and spatial working memory (WM) tasks while their PFC activity was measured using optical topography, a non-invasive, low-constraint neuroimaging tool. Correlation analysis showed that the level of negative mood was inversely associated with PFC activity during the verbal WM task, which replicated our previous findings. Furthermore, the negative correlation between negative mood and PFC activity remained significant after controlling for participants' personality traits, suggesting that natural mood is an independent contributing factor of PFC activity during verbal WM tasks.

1. Introduction

Over the past decades, psychologists have shown that many cognitive processes, such as working memory (WM), are closely related to a person's subjective mood (Mitchell and Phillips, 2007). Neuroimaging studies have begun to elucidate the underlying brain mechanisms, which have implicated the prefrontal cortex (PFC) as a key region responsible for the mood–cognitive interaction (Pessoa, 2008). For instance, a functional magnetic resonance imaging (fMRI) study showed that dorsolateral PFC activation during an N-back working memory (WM) task was decreased when negative mood was induced by the viewing of aversive film clips (Qin et al., 2009). Another fMRI study reported that PFC activity during WM tasks (using words and faces as stimuli) was modulated by positive and negative mood inductions in a stimulus-specific (words vs. faces) manner (Gray et al., 2002). Although some studies have demonstrated how brain activations related to cognitive processes are affected by emotions using cognitive tasks involving emotional stimuli (e.g., emotional Stroop tasks), they did not directly focus on the interaction between mood and WM (Canli et al., 2004; Herrington et al., 2005). Thus, the relationship between mood and PFC activity during WM tasks is still worth investigating.

While most neuroimaging studies examined the mood–cognition interaction using laboratory-based mood-induction procedures, it should be noted that experimentally induced and natural moods in our daily lives are not necessarily identical. Experimentally induced moods are qualitatively different from natural mood in many aspects such as intensity, stability, and persistency (Rusting, 1998; Sison and Mather, 2007). It has been argued that experimentally induced moods tend to be more intense than natural mood (Sison and Mather, 2007). Induced moods are also susceptible to demand characteristics (Sison and Mather, 2007; Westermann et al., 1996), which may involve an emotion-regulation process (Ochsner and Gross, 2005); therefore, they would have different influences on cognition than natural mood. Moreover, experimentally induced moods are typically elicited by viewing or listening to ~10 min of emotional stimuli (e.g., film clips and music) and rapidly disappear after the experiment (Qin et al., 2009). Thus, they usually have acute

* Corresponding author. Tel.: +81 49 296 6111; fax: +81 49 296 5999.
E-mail address: hiroki.sato.ry@hitachi.com (H. Sato).

0925-4927/$ - see front matter © 2012 Elsevier Ireland Ltd. All rights reserved.
http://dx.doi.org/10.1016/j.pscychresns.2012.10.009

effects on cognition. On the other hand, natural mood is formed in daily life and often lasts much longer (hours to days or weeks). Indeed, experimentally induced moods and natural moods sometimes exert completely opposite effects on cognitive performance (Parrot and Sabini, 1990). In recent neuroimaging research using optical topography (OT) (Maki et al., 1995), which can measure brain activity under natural circumstances (e.g., sitting on a chair in an office or living room), researchers have focused on the relationships between natural mood and PFC activity during cognitive tasks. For example, Suda et al. (2009) showed that individuals who reported higher levels of psychological fatigue in daily circumstances exhibited lower levels of PFC activation during a verbal fluency task (VFT). A study from our group also showed that natural variations in negative mood among healthy adults are inversely correlated with PFC activity during a verbal WM task (but not during a spatial WM task) (Aoki et al., 2011). Here, we define the WM as "the temporary retention of information that was just experienced but no longer exists in the external environment" (D'Esposito, 2007), and use simple delayed response tasks. These studies have demonstrated that the PFC plays an important role in the interaction of natural mood and cognition, extending the findings of fMRI studies that relied on experimentally induced moods.

One important limitation of these OT studies, however, is that none controlled for personality differences among participants. Personality traits of individuals are known to affect natural mood in daily lives (Gable et al., 2000) and to be associated with PFC activity during cognitive tasks including WM (Gray and Braver, 2002; Kumari et al., 2004). Thus, observed correlations between natural mood and PFC activity can be "spurious relationships" that just indirectly reflect the associations between personalities and PFC activity. To show that natural moods may be an independent contributing factor of PFC activity during cognitive tasks, one should separate the relationship of natural mood with PFC activity from that of personality.

In this study, we investigated whether the relationship between natural mood and PFC activity during cognitive tasks is explained by personality differences. First, we intended to replicate our previous findings: natural variations in the negative mood levels of healthy adults (as indicated by the scores of the Profiles of Mood States [POMS]) were inversely correlated with PFC activity during a verbal WM task, but did not correlate with PFC activity during a spatial WM task (Aoki et al., 2011). The POMS is a self-report questionnaire that is suitable for evaluating individuals' natural moods in their current life situations (Aoki et al., 2011; Canli et al., 2004; McNair and Heuchert, 2003). Next, we examined whether and how the correlation between natural mood and PFC activity would change after the effects of personality were partialled out. We focused on two sets of personality variables: Neuroticism and Extraversion measured using the NEO Five-Factor Inventory (NEO-FFI) (Costa and McCrae, 1992), and the Behavioral Inhibition System (BIS) and Behavioral Activation System (BAS) measured using the BIS/BAS scales (Carver and White, 1994). These measures have often been used to investigate the relationships between personality and brain activity (Canli, 2004; Canli et al., 2004; DeYoung et al., 2009; Gray and Braver, 2002).

2. Methods

2.1. Participants

Forty healthy adults (10 females, 30 males; mean age=38.4 yr, S.D.=7.4 yr, and range=25–52 yr) participated in this study. Three males were left-handed as determined by the Edinburgh Handedness Inventory (Oldfield, 1971), while the other 37 participants were right-handed. Inclusion or exclusion of the left-handed participants did not affect the main findings reported in this article. Of note, none had participated in our previous study (Aoki et al., 2011); thus, the sample was completely independent. The study was approved by the Ethics Committee of Hitachi, Ltd. All participants provided written informed consent prior to participation.

2.2. Mood and personality measures

Natural moods of the participants were assessed using a short form of the Japanese version of the POMS (Yokoyama et al., 1990). The participants rated 30 mood-related adjectives on a 5-point scale ranging from 0 ("not at all") to 4 ("extremely") on the basis of how they had been feeling during the past week (McNair et al., 1971; Yokoyama et al., 1990). While the POMS has six mood subscales (tension, depression, anger, vigor, fatigue, and confusion), the positive mood score (Pos: the score for the vigor subscale) and the negative mood score (Neg: the sum of the scores for the other five subscales) were used in the analysis, as in previous studies (Aoki et al., 2011; Canli et al., 2004).

Personality was assessed using the Japanese version of the NEO-FFI (Shimonaka et al., 1999) and the BIS/BAS scales (Takahashi et al., 2007). The NEO-FFI is a 60-item self-report questionnaire that assesses the "Big Five" personality traits (Neuroticism, Extraversion, Openness, Agreeableness, and Conscientiousness) (Costa and McCrae, 1992). We particularly focused on Neuroticism and Extraversion, because these two personality variables have been extensively studied for their neurobiological substrates (Canli, 2004; Canli et al., 2004). The BIS/BAS scales consist of 20 statements describing how a person reacts to potentially punishing or rewarding events. The participants rated each item on the basis of how much it held true for them using a 4-point scale (1=does not hold true; 4=holds true) (Carver and White, 1994; Takahashi et al., 2007).

2.3. WM tasks

The tasks were presented through the Platform of Stimuli and Tasks (software developed by Hitachi Ltd., Central Research Lab.). The participants performed two types of WM task (verbal and spatial), each of which had two load (two- and four-item) conditions. Thus, four task conditions were included in total: Verbal/2 items, Verbal/4 items, Spatial/2 items, and Spatial/4 items.

The WM tasks had a delayed-response paradigm (Fig. 1A). Each trial started with a 1500-ms presentation of the target stimuli (S1), which was followed by a delay of 7000 ms. A probe stimulus (S2) was then presented for 2000 ms or until the participant made a response. The inter-trial interval was determined such that the duration between the S2 onset of a trial and the S1 onset of the next trial was randomized between16 and 24 s. We expect that this randomization of the inter-trial intervals reduces the influence of participants' anticipations toward the task onset and spontaneous low-frequency oscillations. Only a fixation cross was presented during the interval and the delay period. A change in the brightness of the fixation cross (500 ms prior to S1 onset) was used as a visual cue for trial onset. Auditory cues, 1000- and 800-Hz pure tones of 100-ms duration, were presented at the onsets of the visual cue and S2, respectively.

In the verbal WM task, two (in the two-item condition) or four (in the four-item condition) Japanese characters in *Hiragana* were presented as S1, and a Japanese character in *Katakana* was presented as S2. *Hiragana* and *Katakana*, syllabaries in the Japanese writing system, represent the same set of syllables with different symbols. The participants indicated by pressing a button whether the character presented as S2 corresponded to any of the characters presented as S1. Because the characters presented as S1 and S2 were presented in different Japanese morphograms (i.e., *Hiragana* and *Katakana*), the participants were prompted to make their judgments on the basis of the phonetic information conveyed by the characters, not on the basis of their form. In the spatial WM task, S1 was the location of two (in the two-item condition) or four (in the four-item condition) white squares out of eight locations, and S2 was the location of a white square. The participant's task was to judge whether the location of the white square presented as S2 was identical to any of the locations of the white squares presented as S1.

2.4. Procedure

Participants completed the POMS questionnaire at the beginning of the experiment. Next, they received computer-automated instructions that were followed by a brief practice session to familiarize them with the tasks. OT measurements were then conducted while the participants performed the WM tasks. The tasks were organized into two sessions, one for the verbal WM task and the other for the spatial WM task, with the order counterbalanced across participants. Each session consisted of 16 trials (eight for each WM-load condition), and sessions were separated by a short break (approximately 1 min). The duration of the OT measurements was approximately 15 min, and the whole experiment took about 45 min. The participants' personalities were assessed after the OT measurement.

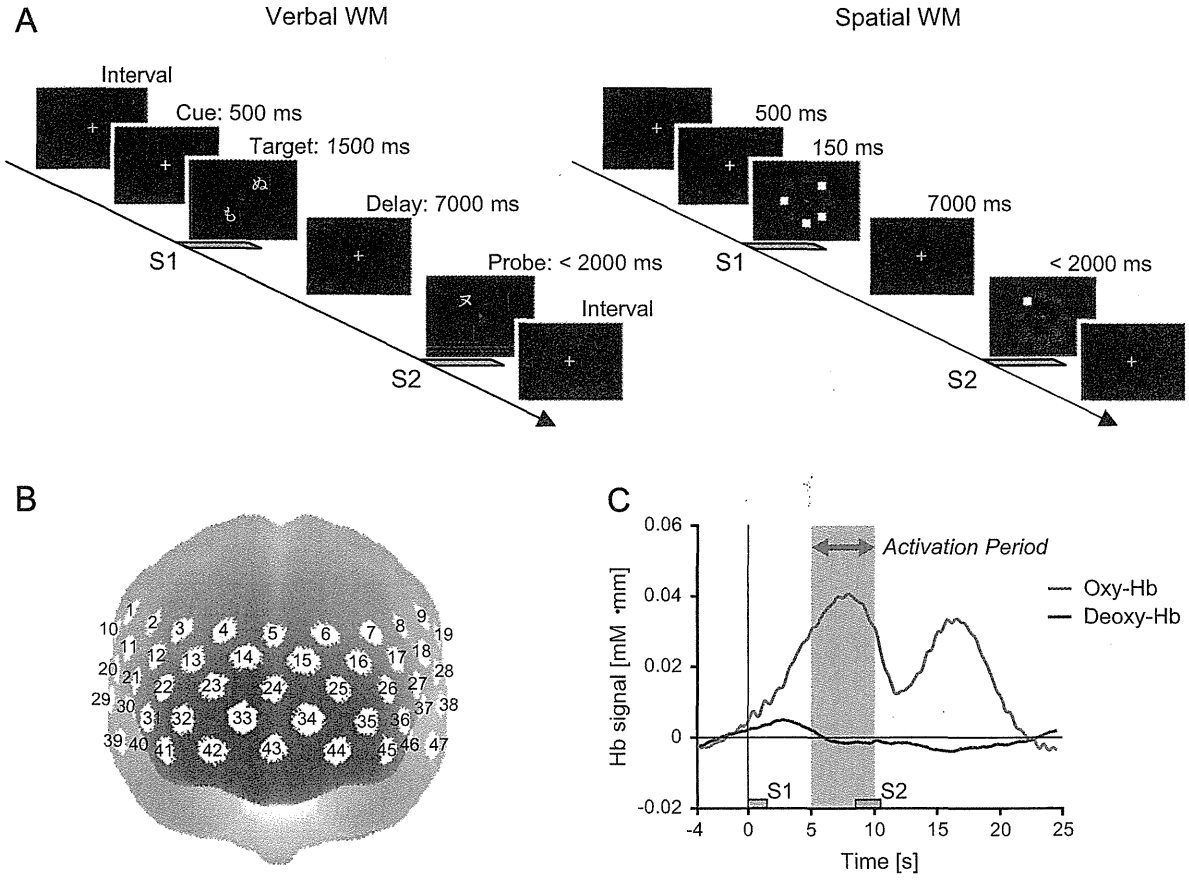

Fig. 1. Task and settings. (A) Schematic diagrams of verbal and spatial WM tasks. Participants were instructed to remember a "target" stimulus (the stimulus to be memorized, S1) and report whether the character (verbal WM task) or location of a white square (spatial WM task) presented in a subsequent "probe" stimulus (the stimulus to be judged, S2) was identical to one of the items in S1. (B) Locations of OT channels (47 measurement points) registered in MNI space based on spatial registration (Singh et al., 2005). (C) Definition of activation period. Graph shows oxy- and deoxy-Hb signal changes during WM tasks for a representative channel (Ch 22), averaged across all blocks, task conditions, and participants. The 5-s activation period (starting 5 s after S1 onset) is indicated by the green rectangle. Gray rectangles indicate time periods for S1 and S2 presentation. (For interpretation of the references to color in this figure legend, the reader is referred to the web version of this article.)

2.5. OT measurement

We used a 47-channel OT system (ETG-7100, Hitachi Medical Corporation, Japan) to measure hemodynamic activity in the PFC. The system uses two wavelengths of near-infrared light (695 and 830 nm), and the relative changes in the oxy- and deoxy-Hb concentrations were calculated on the basis of the modified Beer–Lambert law (Maki et al., 1995). A 3 × 10 probe set consisting of 30 optodes (15 near-infrared light sources and 15 detectors), with an inter-optode distance of 30 mm, was placed on the participant's forehead. This configuration formed 47 measurement points (i.e., channels [Chs]), each one corresponding to a source–detector pair (Fig. 1B). The average power of each light source was 2 mW (for both wavelengths), and the sampling rate was set to 10 Hz.

To estimate the locations of the OT channels in the Montreal Neurological Institute (MNI) space, we used a spatial registration method (Okamoto and Dan, 2005; Singh et al., 2005). The three-dimensional coordinates of the 30 optode locations and scalp landmarks (based on the international 10–20 system: Fp1, Fp2, Fz, T3, T4, C3, and C4) were recorded for 11 volunteers using a 3D-magnetic space digitizer (3D probe positioning unit for OT system, EZT-DM101, Hitachi Medical Corporation, Japan). These data were input to an algorithm (downloaded from http://www.jichi.ac.jp/brainlab/tools.html) and used to estimate the MNI coordinates of the 47 OT channels. Probabilistic anatomical labeling based on the Talairach Daemon database (Lancaster et al., 2000, 2007) was also performed for each OT channel (Okamoto et al., 2009). The results of the spatial registration were used to create activation/correlation maps.

2.6. Data analysis

Analysis was performed using the plug-in-based software Platform for Optical Topography Analysis Tools (developed by Hitachi Ltd., Central Research Lab.) run on MATLAB (The MathWorks, Inc., USA). We mainly analyzed the oxy-Hb signal because previous studies indicated that the contrast-to-noise ratio for the oxy-Hb signal is higher than that for the deoxy-Hb signal (Sato et al., 2011b; Strangman et al., 2002). Indeed, a number of previous OT studies investigating PFC activity during cognitive tasks have focused exclusively on the oxy-Hb signal (Kopf et al., 2011; Ruocco et al., 2010). The time-continuous data of Hb (both the oxy- and deoxy-Hb) signals recorded during a session were divided into 28.5-s task blocks, such that each block consisted of a 4-s pre-task period (starting 4 s before the S1 onset), an 8.5-s task period (during the 1.5-s S1 presentation and the 7-s delay period), a 12-s recovery period (starting immediately after S2 onset), and a 4-s post-task period. Blocks containing an oxy-Hb signal change larger than 0.4 mM• mm over two successive samples (200-ms period) were discarded on a channel-by-channel basis, which provided an objective criterion for rejecting data contaminated by motion artifacts (Aoki et al., 2011; Sato et al., 2011a). The Hb signals of the remaining blocks were smoothed with a 5-s moving average and baseline-corrected by linear regression based on the least squares method using the data from the pre-task and post-task periods of each block.

To evaluate an individual's PFC activation in response to the WM tasks, we calculated 'activation values' for each task condition in a channel-wise manner with the same method used in our previous study (Sato et al., 2011a). First, a 5-s 'activation period' (starting 5 s after S1 onset, taking into consideration the delay of hemodynamic responses to neuronal activity) was determined as the time window of interest. The window included the peak of the oxy-Hb signal increase during the task block (Fig. 1C). The mean oxy-Hb signal values (expressed in mM• mm) during the activation and pre-task periods (defined as above) were calculated for each block. The differences between these values (i.e., the oxy-Hb signal values during the activation period minus those during the pre-task period) were averaged across blocks and divided by the standard deviations (across blocks) to take into account the trial-to-trial variability (Sato et al., 2011a).

In the subsequent group analysis, we performed channel-wise statistical tests on the activation values. Significant PFC activation at the group level for each task condition was assessed by using one-sample t tests of the activation values (vs. zero). The differences in PFC activation across task conditions were evaluated using two-way repeated-measures analysis of variance (ANOVA) of the activation values with the WM types (verbal, spatial) and the WM loads (two items, four items) as within-subject factors. To analyze the relationships between mood, personality, and PFC activity (and also task performance), we calculated correlation coefficients between the questionnaire scores, behavioral measures (accuracy and reaction time [RT]), and activation

values for each task condition. We used the Spearman rank correlation because the relationships between questionnaire scores and behavioral or neural measures are not necessarily regarded as linear (Schroeter et al., 2004). To examine whether the correlations were influenced by confounding factors such as age, gender, handedness, and task performance (both accuracy and RT), we also performed partial correlation analysis. Performance measures were included as control variables because task performance could be related to PFC activity (higher task performance tended to be associated with greater PFC activation, particularly for the spatial WM task: see Supplementary Table S1 and Fig. S1). In these channel-wise analyses, we used the false discovery rate (FDR) method to correct for multiple comparisons among the 47 channels (Singh and Dan, 2006). The false discovery rate (FDR) threshold was set to 0.05 for each topographical map in order not to report more than 5% false positives (on average). We also used permutation tests to calculate "map-wise" *P*-values (Groppe et al., 2011), which indicate the probabilities associated with the following null hypothesis (H_0): "there is no significant correlation between the POMS scores and PFC activity during the WM task in any of the 47 channels consisting of an OT map." We set the "test statistics" as the number of channels, in a map consisting of 47 channels, whose uncorrected *P*-values (determined by the channel-wise Spearman correlation analysis) were lower than 0.05. Under the null hypothesis, the value of the test statistics is expected to be 2.35 (=5% of 47 channels) on average and follow a Poisson distribution due to false positives. For each map-wise test, we performed 10,000 permutations of the POMS scores of participants and computed the test statistics for each permuted data set to generate a distribution of the test statistics (see Supplementary Fig. S2). By comparing the value of the test statistics for the actual (non-permuted) data with this distribution, we obtained a map-wise *P*-value. Permutation tests can successfully control the familywise error rate and automatically adjust to the degree of correlation between multiple tests (Groppe et al., 2011). Thus, they are particularly suitable for the analysis of multi-channel OT data (Singh and Dan, 2006).

We performed several additional analyses to examine the correlations between the POMS scores and other measures of PFC activation. First, we checked if the differences in the oxy-Hb signal changes between the two-item and four-item conditions (4 items−2 items), as well as the sums of the oxy-Hb signal changes between the two conditions (2 items+4 items), were correlated with the POMS scores. Second, we tested whether the second peak of the oxy-Hb signals during the WM tasks (Fig. 1C) correlated with the POMS scores. Third, we tested whether the correlations between the POMS scores and the deoxy-Hb signal during the first and second peaks were significant. These results are reported in Supplementary Tables S2 and S3.

3. Results

3.1. Mood and personality scores

The mood and personality scores of participants are shown in Table 1. The distributions of these scores matched those obtained from the Japanese normative samples (Shimonaka et al., 1999; Takahashi et al., 2007; Yokoyama et al., 1990).

Correlations between mood and personality scores are shown in Table 2. Significant correlations were observed between the Pos and Extraversion scores ($rho=0.61$, $P<0.001$) as well as the Pos and BAS scores ($rho=0.55$, $P<0.001$). Similarly, significant correlations were observed between the Neg and Neuroticism scores ($rho=0.50$, $P=0.001$) as well as between the Neg and BIS scores ($rho=0.44$, $P=0.004$).

3.2. Task performance

The accuracy and RT data are shown in Table 3. Two-way repeated-measures ANOVA was used to examine the effects of WM type (verbal/spatial) and WM load (2 items/4 items) on task performance. A significant main effect of WM load on RT ($F=77.9$, $P<0.001$) was observed, which indicates slower responses under the higher WM-load conditions (i.e., 4 items). A significant main effect of WM type ($F=7.15$, $P=0.011$) and a significant WM-type × WM-load interaction ($F=4.42$, $P=0.042$) were also observed, suggesting that the participants took longer to perform the verbal WM task than the spatial one. The WM-load effects on RT (RTs in the 4-item conditions minus those in the 2-item conditions) were larger for the spatial WM task (99.9 ms for the verbal WM task and 174.6 ms for the spatial WM task; $t=2.10$, $P=0.042$; paired *t*-test). This was due to the RT difference in the 2-item conditions between the verbal and spatial WM task ($t=3.86$, $P<0.001$; paired *t*-test). RTs in the four-item conditions were not different between the tasks ($t=1.13$, $P=0.266$; paired *t*-test). The main effects and the interaction were not significant for accuracy ($F<2.47$, $P>0.124$), which was possibly due to the ceiling effect (especially for the WM-type main effect).

Table 1
Basic statistics for mood and personality scores.

Factors	Mean	S.D.	Range
Mood			
Pos	7.3	3.7	0–14
Neg	29.2	17.0	2–87
Personality			
Neuroticism	23.2	6.6	7–37
Extraversion	24.4	6.3	14–37
BIS	18.5	3.6	10–25
BAS	37.7	5.1	28–52

Note: Pos: POMS positive mood scores; Neg: POMS negative mood scores.

Table 2
Correlations between mood and personality scores.

Factors	Pos	Neg	Neuroticism	Extraversion	BIS	BAS
Mood						
Pos	–					
Neg	−0.32*	–				
Personality						
Neuroticism	−0.11	0.50**	–			
Extraversion	0.61**	−0.39*	−0.27	–		
BIS	−0.27	0.44**	0.58**	−0.36*	–	
BAS	0.55**	−0.36*	−0.16	0.53**	−0.22	–

Note: Pos: POMS positive mood scores; Neg: POMS negative mood scores. All values are Spearman's rank correlation coefficients.

* $P<0.05$; uncorrected.
** $P<0.005$; uncorrected.

Table 3
Task performance.

Task conditions		Accuracy (%)		RT (ms)	
		Mean	S.D.	Mean	S.D.
Verbal WM	2 items	96.9	6.8	1235	200
	4 items	95.6	9.2	1335	211
Spatial WM	2 items	95.3	10.5	1116	186
	4 items	93.1	8.9	1291	255

3.3. Group average of PFC activity during WM tasks

The PFC was reliably activated in response to the WM tasks, as shown in the group-level activation maps (Fig. 2A) and the time courses (Fig. 2B). One-sample *t* tests of the activation values (calculated as described in Section 2 (Methods)) showed significant increases in the oxy-Hb signal during the activation period of the WM tasks for all conditions ($t>2.29$, FDR <0.05). Two-way repeated-measures ANOVA revealed a main effect of WM-load on the activation values for eight channels (Chs 4, 5, 6, 7, 22, 24, 41, 43; $F>8.07$, FDR <0.05), confirming greater PFC activation under higher WM-load conditions. Neither a significant WM-type main effect ($F<9.40$, FDR >0.05) nor a WM-type × WM-load interaction ($F<8.96$, FDR >0.05) was observed.

The overall activation patterns and the locations of activation foci (channels for which the activation values were greatest) were highly similar across task conditions, as shown in Fig. 2A.

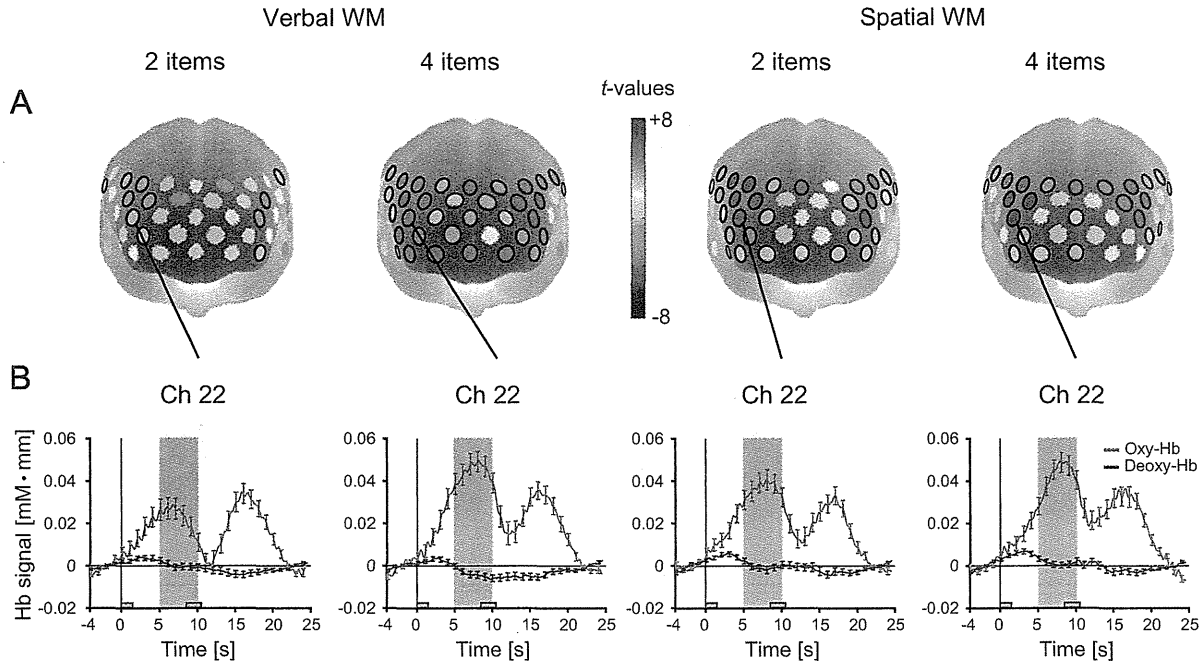

Fig. 2. Hb-signal changes during verbal and spatial WM tasks. (A) Activation maps showing oxy-Hb signal changes in response to the WM task for each task condition. Color scale indicates Student's *t* values (one-sample *t* tests of activation values vs. zero) for each channel. Channels with significant *t* values (FDR < 0.05) are circled with a bold black line. (B) Time courses for oxy- and deoxy-Hb signal changes for a representative channel (Ch 22), representing grand average (with standard error bars) across all participants. Green rectangles indicate activation periods.

To examine the similarity of PFC activation patterns across task conditions, we calculated the correlations between the activation values for any two task conditions on a channel-by-channel basis (see Supplementary Table S4). The activation values between different task conditions were highly correlated (median $rho > 0.42$, $P < 0.007$), especially between the conditions within each WM type (median $rho > 0.54$, $P < 0.001$).

3.4. Relationships between mood scores and PFC activity

The relationships between the POMS scores (i.e., Pos and Neg) and PFC activity for the WM tasks were examined using correlation analysis performed on a channel-by-channel basis (Fig. 3; see also Supplementary Table S1).

The Pos scores were not significantly correlated with activation values for any task condition (map-wise $P > 0.304$, permutation test). However, the correlation between the Neg scores and the activation values for the Verbal/4-item condition was significant (map-wise $P = 0.018$, permutation test). The strongest correlation was observed in Ch 34 ($rho = -0.48$, FDR = 0.07; see Fig. 4), which was located in the anterior PFC (BA 10) as estimated using the spatial registration method (Lancaster et al., 2007; Okamoto et al., 2009; Tzourio-Mazoyer et al., 2002). When we used *P*-values derived from one-tailed tests on the ground of our *a priori* hypothesis that the Neg scores would be negatively correlated with the PFC activity during the verbal WM task, nine channels survived the FDR-corrected threshold (Chs 3, 13, 22, 23, 24, 32, 33, 34, and 43; $rho = -0.48$ to -0.39, FDR < 0.05). Moreover, when we controlled for several confounding variables (age, gender, handedness, accuracy, and RT), significant correlations were found for five channels (Chs 24, 33, 34, 35, and 43; $rho = -0.62$ to -0.47, FDR < 0.05). These channels comprised a "cluster" located in the anterior PFC. In contrast, no significant correlation was found between the Neg scores and the activation values for the other task conditions (map-wise $P > 0.115$, permutation test). Critically, the correlations between the Neg scores and activation values for the Verbal/4-item condition were still significant for 18 channels after the Neuroticism and Extraversion scores were included as additional controlling variables (Chs 3, 4, 9, 13, 15, 23, 24, 25, 26, 33, 34, 35, 40, 41, 42, 43, 44, 45; $rho = -0.65$ to -0.43, FDR < 0.05). Significant correlations also survived in four channels when we controlled for the BAS and BIS scores in addition to age, gender, handedness, accuracy, and RT (Chs 24, 33, 34, and 35; $rho = -0.55$ to -0.50, FDR < 0.05). Larger range and standard deviation of the Neg score (Table 1) did not account for these results, because similar results (i.e., significant correlations after controlling for personality effects) were obtained for the POMS fatigue subscale, whose range and standard deviation were comparable with other mood and personality variables (see Supplementary Fig. S3).

We also examined whether activation differences between the two-item and four-item conditions for the WM tasks were associated with the POMS scores. For this purpose, we calculated correlations between the differences in the activation values (the 4-item conditions minus 2-item conditions) and the POMS scores. However, there was no significant correlation in any condition, either between Pos or Neg scores (map-wise $P > 0.164$, permutation test; see Supplementary Table S2).

3.5. Relationships between personality scores and PFC activity

We also examined the correlations between personality scores and PFC activity. Among the four personality variables, no significant correlation was observed in any task condition (map-wise $P > 0.054$, permutation test), with an exception of the correlation between the BAS scores and PFC activity for the Verbal/2-item condition (map-wise $P = 0.006$, permutation test; Ch 25; $rho = 0.55$, FDR < 0.05). Moreover, this correlation was no longer significant when mood scores (the Pos and Neg) and the other confounding variables (age, gender, handedness, accuracy, and RT) were controlled for (map-wise $P = 0.085$, permutation test). Thus, we found no evidence for a direct relationship between personality and PFC activity independent of participants' moods.

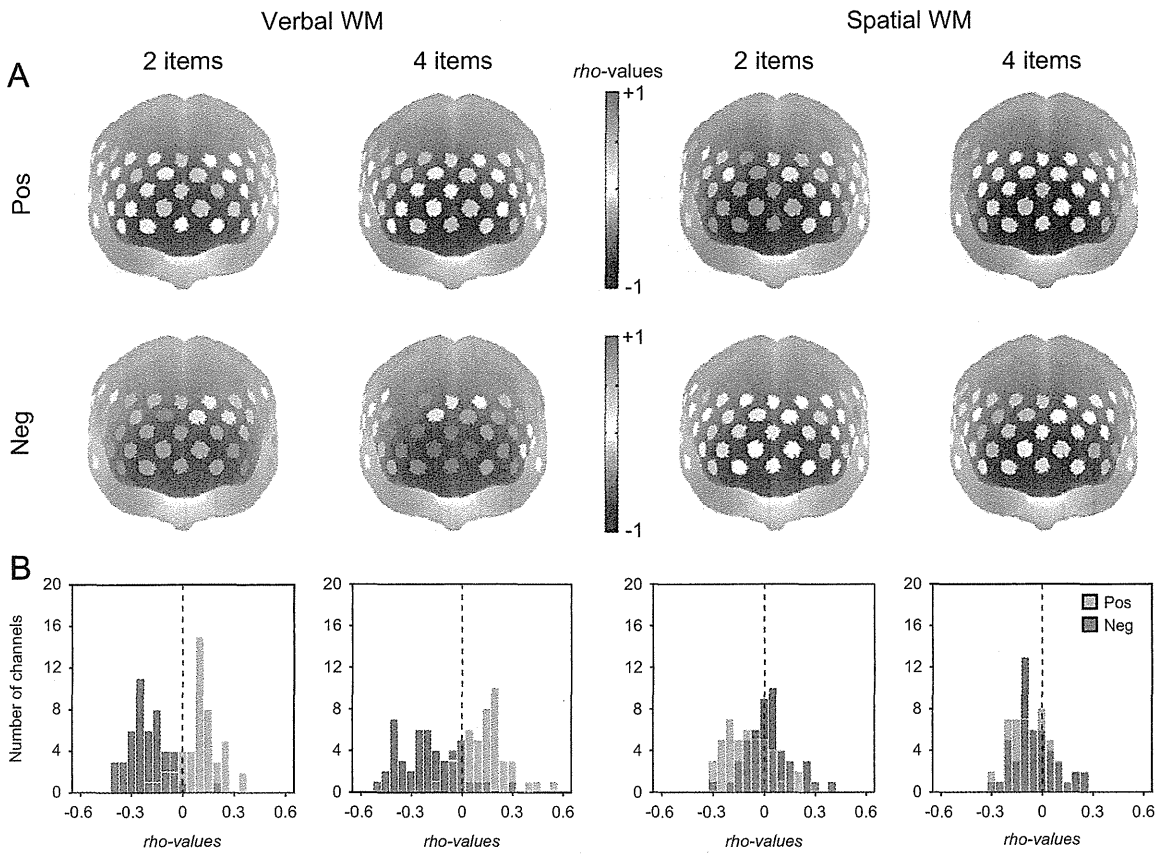

Fig. 3. Relationships between mood and PFC activity. (A) Correlation maps showing relationships between POMS positive or negative mood (Pos and Neg) scores and activation values for each task condition. Color scale indicates Spearman's *rho* values for each channel. (B) Histograms showing distributions of *rho* values for each correlation map, indicating overall tendencies of correlation between mood measures and PFC activity.

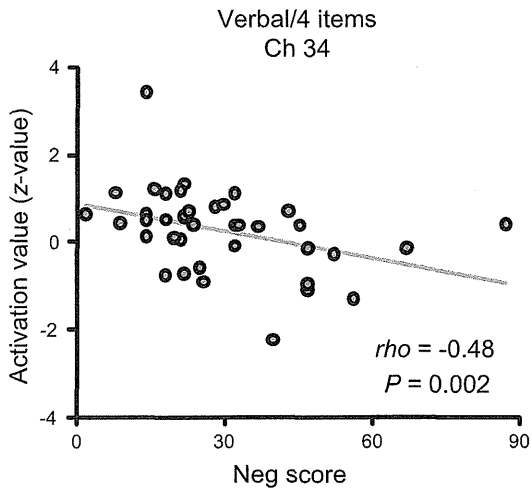

Fig. 4. Correlation plot of mood scores with PFC activity. Negative correlation between individuals' Neg scores and activation values for the Verbal/4-item condition. Plot shows the relationship for the channel with the lowest *rho* value (Ch 34).

4. Discussion

Our aim of this study was to clarify the relationship between natural mood and PFC activity while controlling for personality differences among individuals. We found that the level of negative mood (as indicated by the POMS negative mood scores) was inversely correlated with PFC activity during a verbal WM task under a high WM-load condition, which was consistent with the results of our previous study (Aoki et al., 2011). Moreover, this relationship remained significant even after controlling for individual differences in personality traits (Neuroticism–Extraversion or BIS–BAS) in addition to other confounding factors (i.e., age, gender, handedness, and task performance). These results suggest that natural negative mood has a unique relationship with PFC activity during verbal WM tasks, which is not attributed to the effects of personality.

4.1. PFC activity during verbal and spatial WM tasks

We observed significant PFC activations during the WM tasks for all task conditions. The activation pattern was highly comparable to those reported in our previous studies using essentially the same tasks (Aoki et al., 2011; Sato et al., 2011a) and to those reported in other OT studies using WM tasks (Ehlis et al., 2008; Schecklmann et al., 2010; Schreppel et al., 2008; Tsujimoto et al., 2004). Moreover, it was consistent with those found in many studies of WM tasks using other neuroimaging modalities such as fMRI and positron emission tomography (Smith and Jonides, 1999; Smith et al., 1996; Wager and Smith, 2003). We also observed a WM-load dependency of PFC activity (i.e., higher activation under a high WM-load condition compared to that under a low WM-load condition) for several channels, as predicted. Taking these findings together, we conclude that OT is suitable for measuring WM-related activity in the PFC.

We found no statistical difference in PFC activity between the verbal and spatial WM tasks. These tasks are thought to induce different PFC activation patterns: verbal WM tasks activate the left PFC relatively more, whereas spatial WM tasks activate the right PFC relatively more (Smith et al., 1996). However, such

laterality-based distinction between verbal and spatial WM tasks remains elusive (Ray et al., 2008). Drawing conclusions from our data concerning the activity difference in the PFC between verbal and spatial WM tasks is difficult because the visual stimuli and task performance were not perfectly matched across the WM types in the present study. Further studies are needed to clarify whether and how verbal and spatial WM functions are associated with differential PFC activation.

Time courses of the hemodynamic responses also replicated the results of our previous studies (Aoki et al., 2011; Sato et al., 2011a). As expected, the oxy-Hb signals increased in response to the presentation of the target stimulus (S1), and they reached maximum during the pre-defined activation period. The oxy-Hb signals increased again after the presentation of the probe stimulus (S2). Such two-peaked temporal activation patterns were similar across all four conditions (Fig. 2B). The two peaks may be associated with the WM processes of encoding/maintenance and retrieval, respectively.

4.2. Negative mood and PFC activity during verbal WM task

Our first aim was to replicate our previous work (Aoki et al., 2011). We found significant negative correlations between the level of negative mood and PFC activity only in the verbal WM task but not in the spatial WM task, despite the fact that group averages of PFC activity were statistically equivalent for these tasks. This result is highly consistent with our previous finding based on a completely independent sample ($n=29$), which also revealed a specific correlation between negative mood and PFC activity during a verbal WM task (Aoki et al., 2011). Such reproducibility of the results across the studies suggests a reliable relationship between negative mood measured with the POMS and PFC activity during the verbal WM task. Furthermore, our results are in agreement with previous OT and fMRI studies, which showed that PFC activity during cognitive tasks is attenuated when the participants have higher levels of negative mood (Qin et al., 2009; Suda et al., 2009).

Note that we did not restrict the correlation analysis to the channels that showed significant activation for the WM tasks. We included all 47 channels to control the sensitivities of the correlation maps with the same multiple comparison adjustments among the 47 channels. This approach can be a useful method to identify individual differences in brain activity as a previous study that focused on individual differences demonstrated correlations in brain regions where significant activations were not found at the group level (Canli et al., 2002).

The difference in the relationships of mood with PFC activity between the verbal and spatial WM tasks is also consistent with previous studies. Behavioral experiments have shown that verbal and spatial cognitive functions are selectively modulated by mood states (Bartolic et al., 1999; Gray, 2001), although underlying brain mechanisms remain to be elucidated. The selective effects of neurotransmitters (e.g., dopamine and serotonin) on mood and cognitive functions possibly mediate such specific interactions between mood and cognition (Ashby et al., 1999; Robbins and Roberts, 2007), which should be clarified in future studies.

The difference between verbal and spatial WM in relation to negative mood has another implication to the present results. While the effect of extracerebral hemodynamic changes (e.g., skin blood flow) should be taken into consideration in interpreting OT data, it is unlikely that the present observation concerning the correlation between negative mood and PFC activity is due to these changes because they cannot account for the task-specific correlation between negative mood and verbal WM tasks.

4.3. Relationship between mood and PFC activity independent of personality effects

Our second aim was to separate the contributing factors of natural mood and personality to inter-individual variations in PFC activity during WM tasks. We assessed both the natural mood and personality of participants and evaluated the effect of each factor using partial correlation analysis. This approach has been used to separate the effects of mood states and personality traits in previous behavioral psychological and neuroimaging studies (Bishop, 2009; Canli et al., 2004; Suhr and Tsanadis, 2007). The correlation between negative mood and PFC activity during the verbal WM task was not attenuated after personality scores were included as control variables, suggesting that the observed relationship between negative mood and PFC activity during the verbal WM task is not an indirect association intervened by personality effects. This extends our previous findings by showing the unique contribution of natural mood on PFC activity, which is not simply attributed to personality differences among individuals.

Another approach for separating the effects of mood and personality is to adopt within-subject design and measure mood and brain activity of the same individuals for multiple occasions (Liston et al., 2009). Using this approach, we recently showed that changes in the levels of depressed mood *within* individuals are negatively correlated with PFC activity during the same verbal WM task (Sato et al., 2011a). This study also demonstrated that the relationship between natural mood and PFC activity is independent of some trait factors, which is in line with the present results.

Although natural mood and personality are closely related, they are psychologically distinctive constructs. While recent growth in "personality neuroscience" has begun to elucidate neurobiological substrates for personality (DeYoung et al., 2009), they might not fully cover the neurobiological substrates for natural mood. For example, the relationships of personality with brain activity may reflect genetic variations among individuals, whereas those of mood may reflect the levels of cortical neurotransmitter concentrations that vary within individuals from time to time. The present results showing the unique relationship between natural mood and PFC activity independent of personality are important for considering the distinction of the neural substrates of mood and personality.

4.4. Limitations

There are some limitations to be discussed in this study. First, the gender ratio in the participants was imbalanced (female:male=1:3). However, we speculate that our finding is not dependent on a gender difference because the partial correlation analysis controlled for gender replicated the results. Moreover, Canli et al. (2004) did not mention any evidence of a fundamental difference between male and female participants in how brain activation is associated with either personality trait or mood state. It might be interesting in the future study to examine gender differences in terms of the relationship between brain activity and mood states with larger and more gender-balanced samples.

Second, we need to consider limitations of our WM tasks. Although we found greater activation values in a high-load (4-item) condition than in a low-load (2-item) condition in eight channels, we did not find significant correlations of the negative mood with the PFC activity related to the contrast between the two load conditions. This might be because the WM-load difference between the two conditions was relatively small. Indeed, the accuracies were not significantly different between the two-item